Spatial variability of diurnal temperature range and its associations with local climate zone, neighborhood environment and mortality in Los Angeles

Shengjie Liu[a], An-Min Wu[a], Hung Chak Ho[b]

[a]*Spatial Sciences Institute, Dornsife College of Letters, Arts and Sciences, University of Southern California, Los Angeles, CA 90089, USA*
[b]*Department of Anaesthesiology, School of Clinical Medicine, LKS Faculty of Medicine, The University of Hong Kong, Pokfulam, Hong Kong*

Abstract

Urbanization alters the Earth's emissivity and leads to intraurban differences in temperature variations, including diurnal temperature range (DTR). Despite DTR as a factor of thermal discomfort and mortality risk worldwide, its spatial variability and intraurban associations with local climate zone (LCZ), neighborhood environment and mortality risk have not been investigated. This study first applied the LCZ framework to evaluate associations between climate-sensitive urban design and long-term DTR exposure in Los Angeles, a megacity with the largest DTR in the United States. Using fine-scale daytime and nighttime Landsat thermal imagery to quantify DTR, we found that compact low-rise areas had high DTR, high-rise areas with moderate DTR, and natural areas with the lowest. Young-age, non-white and low-income populations were vulnerable and exposed to high DTR. A spatial Bayesian Poisson regression confirmed that neighborhoods with higher DTR exhibited higher mortality risk after controlling for socioeconomic factors (relative risk: 1.047, 95% credibility interval 1.013-1.082). We did not observe a significant association between mean temperature and mortality in our study. As spatial variability of DTR induces heterogeneous exposure and the evidence that long-term DTR exposure is positively associated with mortality across neighborhoods, planners and policymakers should consider urban landscaping to mitigate large DTR for risk reduction.

Keywords: diurnal temperature range, local climate zone, neighborhood environment, spatial variability, all-cause mortality, built environment

1. Introduction

More than 55% of the world's population live in cities, where people gather and come with pollution and heat (Kuznets, 1955; Dinda, 2004). Cities have various spatial patterns and structures, such as regular-gridded dense high-rise (e.g., New York) and vastly sprawl low-rise-dominant (e.g., Los Angeles), and different types of city design can affect spatial variability of local temperature variously. Building density, building height, and urban landscaping including green space – these are parts of the elements that lead to different local temperature illustrated in the established local climate zone (LCZ) system (Stewart and Oke, 2012). Even within a small city, temperature heterogeneity exists, and this spatial heterogeneity can affect mortality risk (Anderson and Bell, 2009). Specifically, spatial heterogeneity of local temperature is often influenced by the local built environment, including ventilation and surface materials (Mirzaei, 2015), city texture (Sobstyl et al., 2018), and heat convection efficiency (Zhao et al., 2014), and it can induce urban heat islands (UHIs), a phenomenon describing higher temperature in urban areas than in rural areas. For example, a study in Wuhan (China) found that urban form metrics (e.g., sky view factor) were the major contributing factors to UHIs (Yin et al., 2018). By using the LCZ framework (Stewart et al., 2014), a standardized classification scheme composed of 17 urban and natural landscape classes for quantifying urban climate patterns, Geletič et al. (2019) found that dense built-up areas had the highest UHI intensity in summer in three central European cities.

---

*Email: liusheng@usc.edu. Address: 3616 Trousdale Pkwy, AHF B55, Los Angeles, CA 90089, USA

The above climate-sensitive urban environment may not only affect average temperature of different neighborhoods, but also influence diurnal temperature range (DTR), daily temperature variation caused by the difference between the daytime maximum and nighttime minimum temperatures (Kan et al., 2007; Lim et al., 2015; Kim et al., 2016). As people can adapt to regional climate and the optimal minimum mortality temperature differs for each city (e.g., 30°C for Bangkok, Thailand vs. 19°C for London, UK), the variation of the local temperature (e.g., DTR) thus plays a vital role on population health (Gasparrini et al., 2015). There exists a body of research showing the association between DTR and mortality/morbidity from Shanghai (Kan et al., 2007), five east-Asian countries (Lee et al., 2017), England and Wales (Zhang et al., 2018), Spain (Ponjoan et al., 2021), the Middle East (Sharafkhani et al., 2017), the US (Lim et al., 2015), and ten countries across the globe (Lee et al., 2018). One particular study by Lim et al. (2015) showed that of the seven regions in the US, Southern California (where Los Angeles is located) was found with the largest DTR and the highest effects of DTR on nonaccidental mortality.

However, despite DTR as a risk factor, most studies only focused on temporal effects but not spatial variability (Cheng et al., 2014). In contrast, studies describing temperature-related mortality at neighborhood levels only examined daily average or maximum temperature without considering temperature variations (Son et al., 2019). There is no study investigating intracity effects of DTR on mortality yet. This is partly because of the scarcity of weather stations. Even in a developed city like Los Angeles, only 24 stations are available from the Automated Surface Observing Systems, compared to a few hundred zip code areas (Muthukumar et al., 2022). Although satellite-derived brightness and land surface temperature data have become more available in recent years, the high learning curve to use remote sensing data by health scientists becomes a major obstacle, as discussed by White-Newsome et al. (2013). White-Newsome et al. (2013), Thorpe et al. (2022), and more experts agree that health science should look into satellite-derived data to tackle environmental justice issues. There are already some studies demonstrating the significant correlations between air temperature and satellite-derived temperature (White-Newsome et al., 2013; Berg and Kucharik, 2021), the validity of using satellite-derived temperature to predict air temperature (Pelta et al., 2016; Pelta and Chudnovsky, 2017; Wilson et al., 2022), and the validity of using satellite-derived temperature for public health research (Johnson and Wilson, 2009; Smargiassi et al., 2009; O'Brien et al., 2020; Sabrin et al., 2020).

As health inequality often occurs in various cities, especially metropolitans in the US, investigating intracity variability of DTR is therefore essential. Particularly, spatial variability of DTR can represent long-term heat exposure in various neighborhoods. Thus, understanding DTR variability and its association with local climate zone, neighborhood environment and mortality risk can help urban planners and health officials build better neighborhoods and tackle social problems for health management. It is critical for people who are vulnerable to temperature variability as they may have limited health and social resources to mitigate temperature extremes (e.g., low affordability to use air conditioning and electricity, low level of information-seeking for health warnings).

Therefore, this study evaluated the spatial variability of DTR and its association with local climate zone, neighborhood environment and mortality in Los Angeles, a megacity in Southern California with the largest DTR in the US. Specific objectives include: 1) application of the LCZ framework to categorize the built environment (high-rise vs. low-rise, compact vs. sparse, etc.) and to quantify its association with local variability of DTR, 2) application of census data to evaluate the relationships between neighborhood environment and DTR variability, and 3) application of a spatial Bayesian Poisson regression to evaluate the association between long-term exposure to various temperature variability (mean temperature and DTR) and all-cause mortality data at the zip code level.

2. Data and Methods

2.1. Data Collection

Annual mortality data (2009-2018) were retrieved from the California Health & Human Services Agency[1], including 850,501 all-cause deaths. These data are the latest data without the interruption of COVID-19. They were death records at the zip-code level. For zip-code areas with less than 11 death counts in a year, the data were censored. California age-specific death rates in 1999-2020 were obtained from the Centers for Disease Control and Prevention (CDC) Wonder. Age-specific death rates and populations in each zip code area were used to calculate the expected death that was used in the model for indirect age adjustment. Within each zip-code area, for the i-th age group of a

---

[1] https://data.chhs.ca.gov/dataset/death-profiles-by-zip-code

2

total of k age groups, the crude death rate is CDR_i, and the population is POP_i. The expected death of this zip-code area can be calculated as

$$E = \sum_{i=1}^{k} POP_i * CDR_i. \qquad (1)$$

Two types of data – (1) socioeconomic data to represent neighborhood environment and (2) built environment data – were extracted for two purposes. The first purpose was to use the census-tract level data to assess the vulnerable populations and places. The second purpose was to use the zip-code level data in the regression model as covariates to assess effects of DTR on mortality.

Socioeconomic data include populations by ethnicity, populations by 5-year age group, median household income, population density calculated from total population and land area, and populations by gender. These socioeconomic data were extracted from the 2015 American Community Survey (ACS) 5-year estimates.

Built environment data of this study included: LCZ, annual mean PM2.5, green space, and building area proportion. LCZ was retrieved from a global product by Demuzere et al. (2022) with a resolution of 100 m and an overall accuracy of 90%. Table 1 describes the details of 17 LCZ classes, including 10 urban categories and seven natural categories (Stewart and Oke, 2012). Among the urban classes, LCZ-1 to LCZ-3 are considered dense urban areas (mostly built-up with limited vegetation), and LCZ-4 to LCZ-6 are considered sparse urban areas (with sufficient vegetation). High-rise is typically over 10 stories tall, mid-rise is 3-9 stories, and low-rise is under 3 stories. Annual mean PM2.5 data were calculated based on the 2008-2018 daily PM2.5 concentrations retrieved from a census-tract and zip-code level dataset for Western US developed by Reid et al. (2021). Mean Normalized Difference Vegetation Index (NDVI) was used to demonstrate the variation of green space. Mean NDVI values were calculated from Landsat-5 imagery in 2009-2012 and Landsat-8 imagery in 2013-2018 in Google Earth Engine. Building area proportion was calculated from OpenStreetMap as of April 2022. We show the spatial data (NDVI, PM2.5, population density) in Figure 1 so that readers can have the context of the study area.

Table 1: Description of Local Climate Zone (LCZ)

Type	Description	Category
LCZ-1	Compact high-rise	Urban
LCZ-2	Compact mid-rise	Urban
LCZ-3	Compact low-rise	Urban
LCZ-4	Open high-rise	Urban
LCZ-5	Open mid-rise	Urban
LCZ-6	Open low-rise	Urban
LCZ-7	Lightweight low-rise	Urban
LCZ-8	Large low-rise	Urban
LCZ-9	Sparsely built	Urban
LCZ-10	Heavy industry	Urban
LCZ-A	Dense trees	Natural
LCZ-B	Scatterred trees	Natural
LCZ-C	Bush, scrub	Natural
LCZ-D	Low plants	Natural
LCZ-E	Bare rock or paved	Natural
LCZ-F	Bare soil or sand	Natural
LCZ-G	Water	Natural

For the first purpose to assess vulnerable populations and places at the census tract level, all the data were used. When demonstrating the DTR exposure across ethnicity and age groups, we used the population-weighted exposure. For example, the population-weighted DTR of Hispanics was calculated by multiplying each neighborhood's DTR by each neighborhood's Hispanic population and then divided by the total Hispanic population. For the second purpose in the regression model to assess effects on mortality at the zip-code level, these socioeconomic and built environment data required further processing to avoid multicollinearity and complicating the model. Specifically,
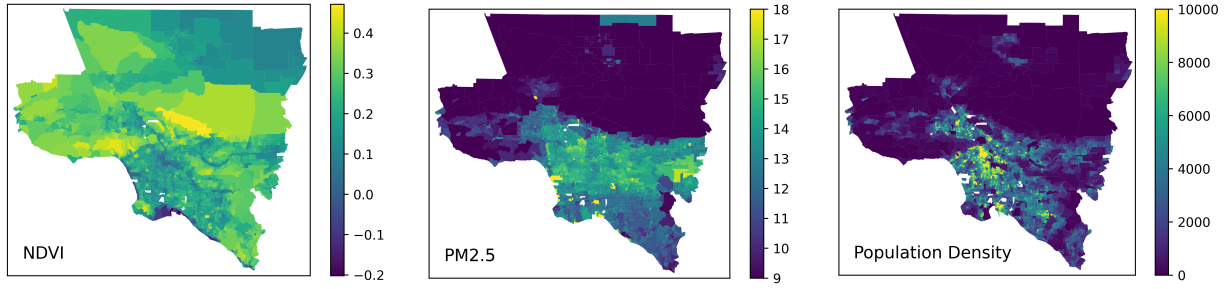
Figure 1: Spatial distribution of NDVI, PM2.5 ($\mu g/m^3$), and population density (per km^3).

only the percentage of age>65 was used in the regression model, as a common practice in environmental health studies to examine older adults – a known vulnerable population (Rosenthal et al., 2014; Shi et al., 2015). Only the percentage of white population was included in the regression, because the percentage of non-white population (often considered vulnerable) is collinear with and the opposite of the percentage of white population.

Annually mean temperature and annual average DTR were used as temperature indicators to quantify temperature variations in this study, as shown in Figure 2. Both were quantified based on Brightness Temperature, a metric referred to as temperature at blackbody and been used in other health studies (Chen et al., 2006; Cao et al., 2008; Yang et al., 2022). In this study, we did not use land surface temperature (LST) 1) due to the lack of nighttime land surface emissivity which is critical to evaluate LST products (Sekertekin and Bonafoni, 2020), and 2) since LST is derived based on land emissivity, thus a comparison between LST and land cover-related products (e.g., LCZ) may have statistical bias because both products were associated with emissivity (Wan and Dozier, 1996; Du et al., 2015; Niclòs et al., 2021). Using Brightness Temperature may avoid this problem. Specifically, two pairs of daytime and nighttime cloudless thermal imagery from four dates were first obtained from Landsat 8 and 9 to estimate temperature variations in Los Angeles (Table 2), including a pair for summer DTR (July 2020) and a pair for winter DTR (February 2022). The Landsat data were downloaded from the United States Geological Survey (USGS, https://earthexplorer.usgs.gov/). Sensitivity analyses were applied to crosscheck data quality for the summer pair. Based on similar temperature profiles of the two dates (July 3 and 18, 2020) of summer Landsat images (Figure 3), the estimation of summer DTR was appropriate. We calculated the annual average DTR in each neighborhood based on the average of summer and winter DTRs. A correlation test was also conducted to validate the use of calculated annual average DTR in modeling. A moderate correlation (r=0.575) was found between the summer and winter DTRs (Figure 4).

Table 2: Acquisition times of the eight scenes from four dates of two seasons.

Season	Date	Local Time
Summer (UTC-7)	2020-07-18 nighttime	10:41:45 PM
		10:42:15 PM
	2020-07-03 daytime	11:28:08 AM
		11:28:31 AM
Winter (UTC-8)	2022-02-06 nighttime	9:42:29 PM
		9:42:53 PM
	2022-02-07 daytime	10:28:35 AM
		10:28:59 AM

2.2. Spatial variability of DTR

We identify the spatial variability of DTR with a *bivariate* local indicator of spatial association (LISA) based on two variables: nighttime and daytime temperatures at the census tract level. Specfically, *bivariate* LISA was proposed by Anselin (1995) for analyzing spatial heterogeneity of two variables, and has been commonly used to identify the vulnerable areas in environmental health studies (Singh et al., 2011; Thach et al., 2015; Ho et al., 2018; Chen et al.,
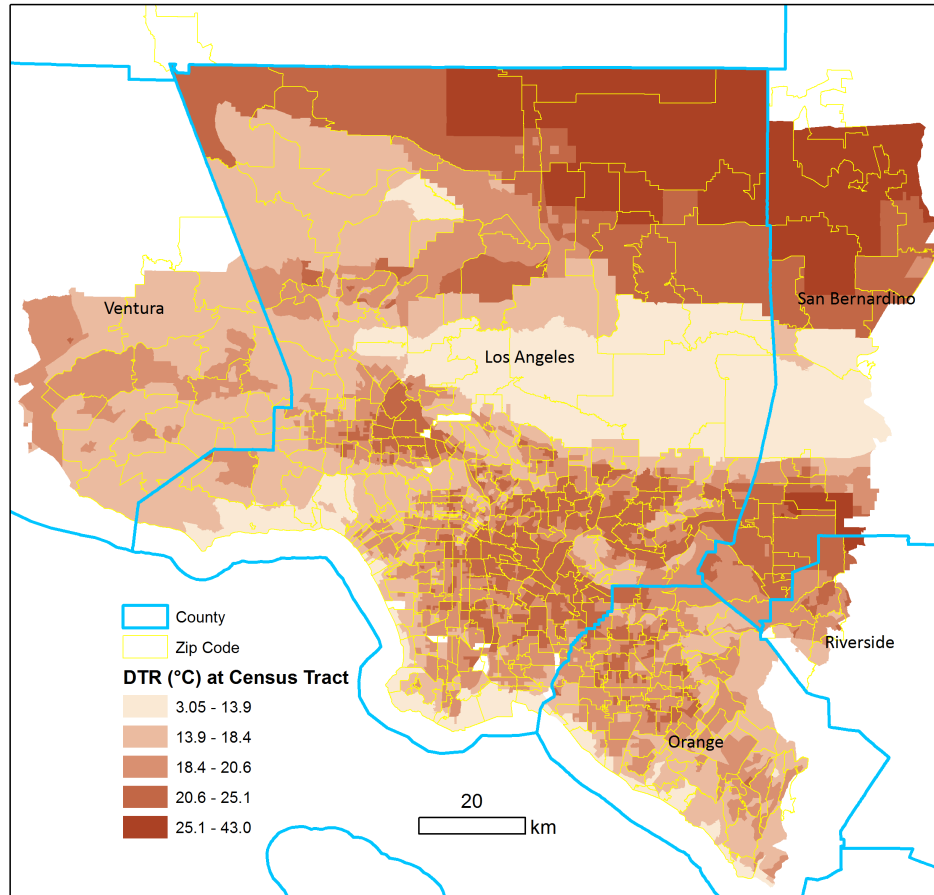
Figure 2: DTR at the census tract scale, overlapped with zip code boundaries (in light yellow). The analysis of DTR's patterns was conducted on census tracts. The effects on mortality was conducted on zip codes.
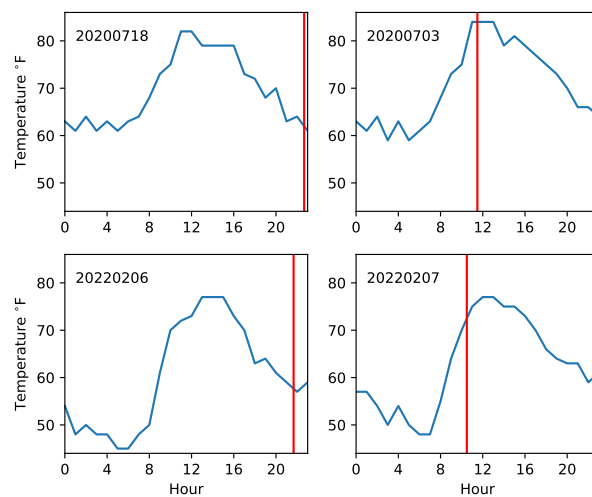

Figure 3: Temperature profiles of the four dates. Red line marks the acquisition time of the satellite imagery. For the summer pair, the calculated DTR is roughly the difference between the maximum and minimum temperatures. For the winter pair, the calculated DTR is an underestimation.
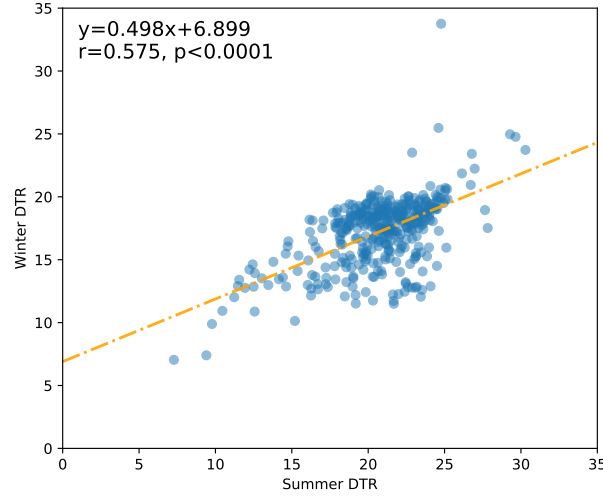
Figure 4: Winter DTR as a function of summer DTR. Overall DTRs in summer and winter show moderate consistency (r=0.575).

2022). Unlike the conventional Moran's I that identifies global spatial dependence, the LISA approach can detect local clusters – which can help us identify vulnerable areas. The *bivariate* LISA in this study is calculated as:

$$I_i = Z_{i,n} \sum_{j=1}^{k} W_{ij} Z_{j,d} \tag{2}$$

where

$$Z_{i,n} = \frac{|x_{i,n} - \bar{x}_n|}{\sigma(x_n)}, \quad Z_{j,d} = \frac{|x_{j,d} - \bar{x}_d|}{\sigma(x_d)} \tag{3}$$

where i is the corresponding location of a census tract; $x_{i,n}$ is the nighttime temperature of this i-th unit; $x_{j,d}$ is the daytime temperature of the neighbored j-th unit; k is the number of neighbored units; $\bar{x}_n$ and $\bar{x}_d$ are the mean nighttime and daytime temperatures, respectively; $\sigma(x_n)$ and $\sigma(x_d)$ are the standard deviations of nighttime and daytime temperatures, respectively; and W_{ij} is the spatial matrix. We adopted queen contiguity as spatial matrix in order to identify data with sharing sides and common vertices neighbors.
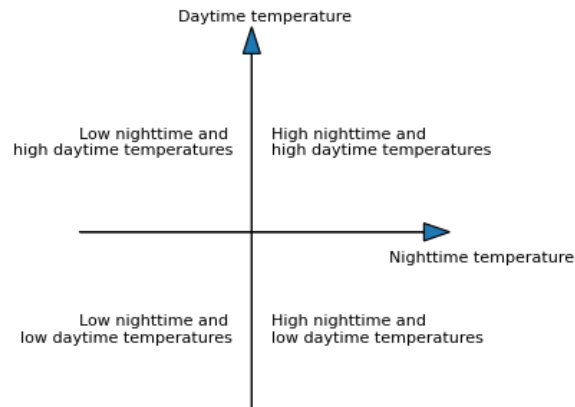

Figure 5: Four quadrants of LISA analysis.

6

Four types of spatial clusters were generated: High-High, Low-Low, High-Low, and Low-High (Figure 5). In this study, nighttime temperature is the first variable and daytime temperature is the second variable in LISA. Specifically, a Low-High unit in this study suggests that it is with a low nighttime temperature but surrounded by units of high daytime temperatures, meaning that it is with a high DTR. A High-Low unit suggests that it is with a high nighttime temperature but surrounded by units of low daytime temperatures, meaning that it is an UHI at night but an urban cool island in the daytime. A High-High unit suggests that it is with high nighttime and daytime temperatures. A Low-Low unit suggests that it is with low nighttime and daytime temperatures. The High-High units are likely to be UHIs, and the Low-Low units are likely to be cool areas such as green space. The *bivariate* LISA was performed in GeoDA (Anselin et al., 2009).

2.3. Spatial associations between DTR, LCZ and neighborhood environment

This study applied a land use/land cover (LULC) analysis to evaluate the spatial associations between DTR and LCZ. In detail, we considered each LCZ class as a land cover and extracted corresponding DTR values of all pixels in 100-m resolution (the resolution of LCZ data) of each class for comparison. Summer and winter DTRs were compared separately. Descriptive statistics were used to compare the DTR range and standard deviation of each LCZ class.

Spatial associations between DTR and neighborhood environment were compared based on a zonal analysis. Specifically, we considered each census tract as a spatial zone and extracted corresponding DTR values of all pixels in 30-m resolution (the resolution of DTR data) in each census tract for comparison. Descriptive statistics were used to compare DTR range of each census tract. We then summarized the population-weighted exposures 1) by age group and 2) by ethnicity. We also summarized the results based on the neighborhood and environment characteristics of census tracts, including median household income, percentage of building area, percentage of female populations, green space (mean NDVI value), PM2.5, and population density.

2.4. Spatial associations between DTR and all-cause mortality

This study applied spatial Bayesian Poisson regression to evaluate the associations between spatial variability of DTR and all-cause mortality. The workflow of the spatial regression is shown in Figure 6, and the study area can be found in Figure 2. Standardized mortality ratio (SMR) was a health outcome to quantify neighborhood-level all-cause mortality. DTR was assigned a binary variable to compare areas with DTR higher or lower than the 50th percentile. Mean temperature, median household income, percentage of age>65 (Age>65 %), percentage of white population (White %), percentage of female population (Female %), annual PM2.5 concentration (PM2.5), mean NDVI (Green Space), population density, and percentage of building area (Building Area %) in zip-code level were assigned as covariates. The specific model was as follows:

$$Y_i \sim Poisson\,(E_i\theta_i) \tag{4}$$

$$ln\,(\theta_i) = \beta_1 + \beta_2 x_i + ... + \beta_p x_{ip} + u_i + v_i \tag{5}$$

where Y_i is the observed death counts and E_i is expected death counts, i is the geographic unit, θ_i was SMR, x_p was covariates, u_i was structured random effect for spatial dependence, and v_i was unstructured random effect for unit-specific heterogeneity. Relative risk (RR) and 95% credibility interval (CrI) were reported in this study. The regression was conducted on R-INLA package of R software.

Additionally, sensitivity analysis was conducted to compare the results of spatial Bayesian Poisson regression with other models: binomial regression, a Bayesian Poisson regression without considering spatial dependence, and a mixed model (García-Pérez et al., 2013; Besag et al., 1991; Leroux et al., 2000). Sensitivity analysis indicated fairly similar results for all models.

3. Results

3.1. Vulnerable areas

After removing areas without DTR data, a total of 389 zip codes and 3213 census tracts were included in the study, covering the entire Los Angeles County and parts of Ventura County, San Bernardino County, Riverside County, and Orange County (natural extensions of the Greater Los Angeles), as shown in Figure 2. In general, UHI effects and
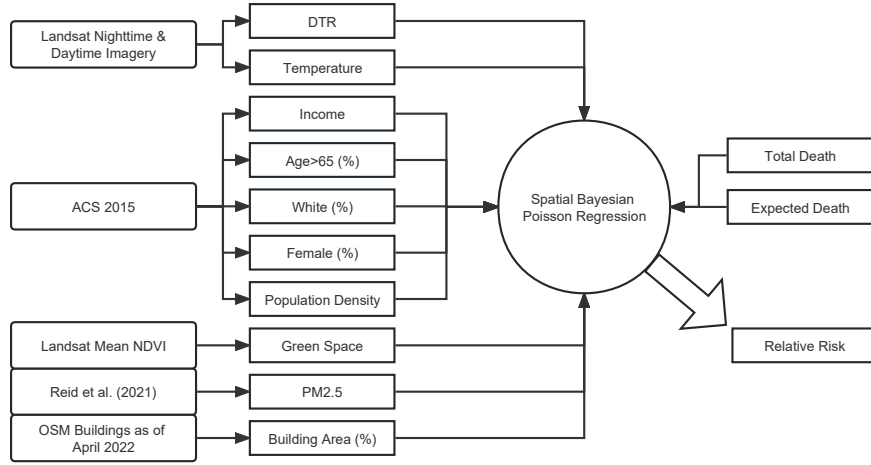
Figure 6: Workflow of the spatial Bayesian Poisson regression. ACS: American Community Survey. NDVI: Normalized Difference Vegetation Index. OSM: OpenStreetMap. DTR: Diurnal Temperature Range.

spatial heterogeneity of DTR variations were observed across Los Angeles. For example, Santa Monica in the west coastal area during August had an average temperature of 70.6°F (21.4°C) versus 78.5°F (25.8°C) of Pasadena, an Inland city in Los Angeles County (Figure 7). DTR was significantly smaller for Santa Monica than for Pasadena.
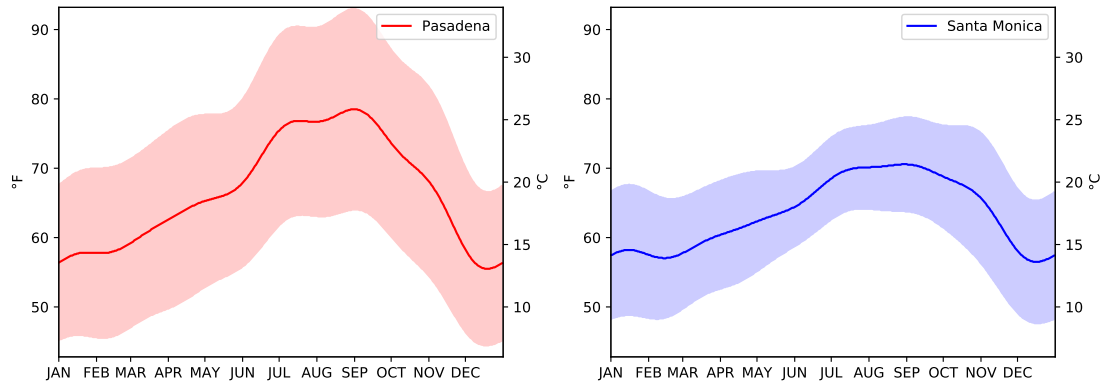

Figure 7: Daily temperatures between 2006-2020 of Pasadena and Santa Monica. Solid line: mean temperature of these years; shaded areas: the range between maximum and minimum temperatures of these years, i.e., diurnal temperature range (DTR).

Based on LISA analysis shown in Figure 8, DTR extremes were clustered in specific areas in winter. Of the 3213 census tracts, 405 were High-High areas (in red), 190 were Low-Low areas (in blue), 367 were Low-High areas (in light blue), and 263 were High-Low areas (in light red). For High-High areas with both high nighttime and daytime temperatures, these were neighborhoods clustered around Inglewood and Hawthorne, along the I-110 freeway, and along the I-5 freeway. Particularly, high temperatures throughout the day in these areas may be associated with UHI. For Low-High areas with low nighttime temperature and high daytime temperature, which indicated large DTR, these were mainly clustering in two neighborhoods – Commerce and Anaheim City of Orange County – and were surrounded by High-High areas. For High-Low areas with high nighttime and low daytime temperature, indicating a small DTR, most of which were on the mountains and close to the ocean.

Summer had a slightly different scenario of spatial clusters in Los Angeles (Figure 8 lower image). Low-Low areas with low temperatures day and night were concentrated along the coast. Three High-High areas in inland areas were identified (from left to right: SFV: San Fernando Valley; SGV: San Gabriel Valley; Ontario, CA). Additionally, there were fewer Low-High areas (with large DTR) compared to winter, and most of these areas were surrounding the
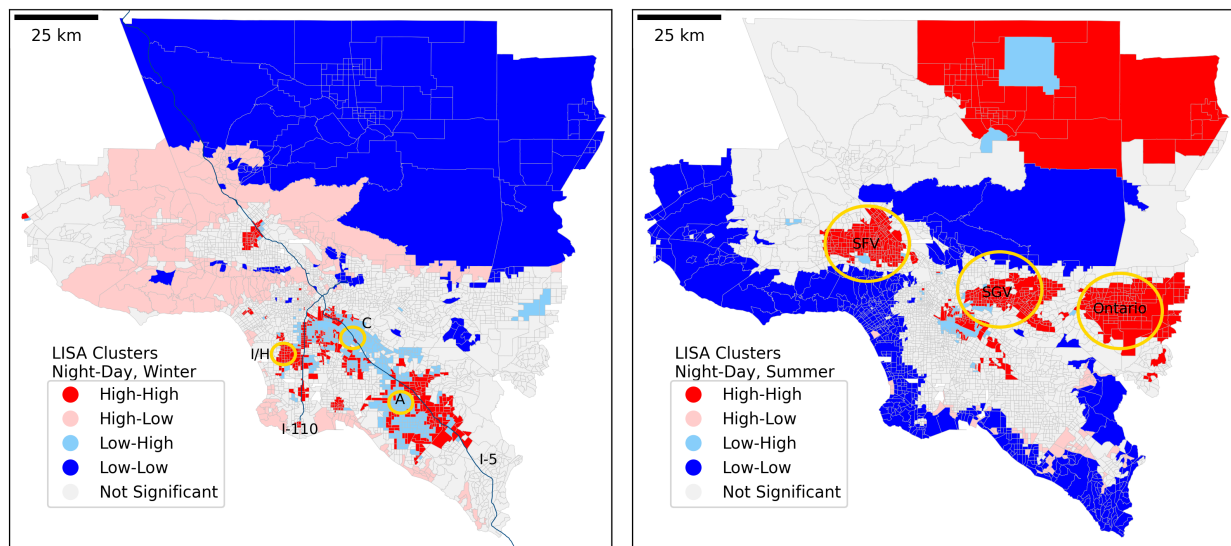
Figure 8: Vulnerable areas identified by LISA statistics (Left: winter; right: summer). X: nighttime temperature, Y: daytime temperature. High-High: high nighttime high daytime temperature (in red, consistently high UHIs). Low-Low: low nighttime low daytime temperature (in blue, consistently low UHIs). Low-High: low nighttime high daytime temperature (in light blue, large DTR). High-Low: high nighttime low daytime temperature (in light red, low DTR). LISA: local indicator of spatial association. I/H: Inglewood and Hawthorne. C: Commerce. A: Anaheim. SFV: San Fernando Valley. SGV: San Gabriel Valley. I-110 and I-5 are highways.

inland High-High areas.

3.2. Association between DTR and LCZ

While sea breeze partly explains the spatial variability of DTR, built environment factors such as building density, height, and green space may also be key determinants. Based on the comparison between spatial variability of DTR and LCZ (Figure 9), in winter, LCZ with a low-rise urban design or with sufficient impervious surfaces showed a larger DTR, e.g., LCZ-3 compact low-rise (17.8°C) and LCZ-8 large low-rise (17.5°C). Within the three compact and three open LCZs, respectively, high-rise showed a lower DTR. LCZ-1 compact high-rise showed a mean DTR of 10.5°C, followed by LCZ-2 compact mid-rise's 14.3°C and LCZ-3 compact low-rise's 17.8°C. The pattern for LCZ-4 to LCZ-6 from high-rise to low-rise was similar, being 14.0°C, 14.6°C, and 16.4°C, respectively. While natural LCZs had a lower DTR in general, LCZ-1 compact high-rise showed a similar low DTR at a higher average temperature.

The patterns of summer and winter are similar, with summer DTR's values larger. Among the three compact LCZs, LCZ-1 compact high-rise had the lowest DTR (17.6°C), followed by LCZ-2 compact mid-rise's 20.1°C and LCZ-3 compact low-rise's 22.2 °C. Among the three open LCZs, LCZ-4 open high-rise had the lowest DTR (17.4°C), followed by LCZ-5's 18.2°C and LCZ-6's 20.9°C. LCZ-G water in both winter and summer is with the lowest DTR. The difference in DTR between urban areas (LCZ-1 to LCZ-10) and the typical natural areas (LCZ-A dense trees) was larger in summer than in winter.

3.3. Vulnerable populations and neighborhood environments

This study also found a high vulnerability caused by DTR among non-white populations (Figure 10). Specifically, with the population-weighted exposure to DTR, Hispanic was found to be exposed to a higher DTR (mean DTR: 20.5°C), followed by Black (20.3°C) and Asian (19.7°C), while the population-weighted exposure to DTR (18.8°C) of white population was the lowest throughout the year. Interestingly, we found higher vulnerability among younger populations but not older populations (Figure 11). Specifically, individuals aged 65-69 and 85+ were exposed to the lowest DTR (19.5°C), whereas individuals aged 0-4 were exposed to the highest DTR (20.1°C).

Census tracts with a lower median household income were exposed to a higher DTR (Figure 12). The mean DTR was 20.6°C for census tracts with a median household income smaller than US$50,000; in contrast, the mean DTR was 17.3°C for census tracts with a median household income larger than US$100,000. As expected, census tracts
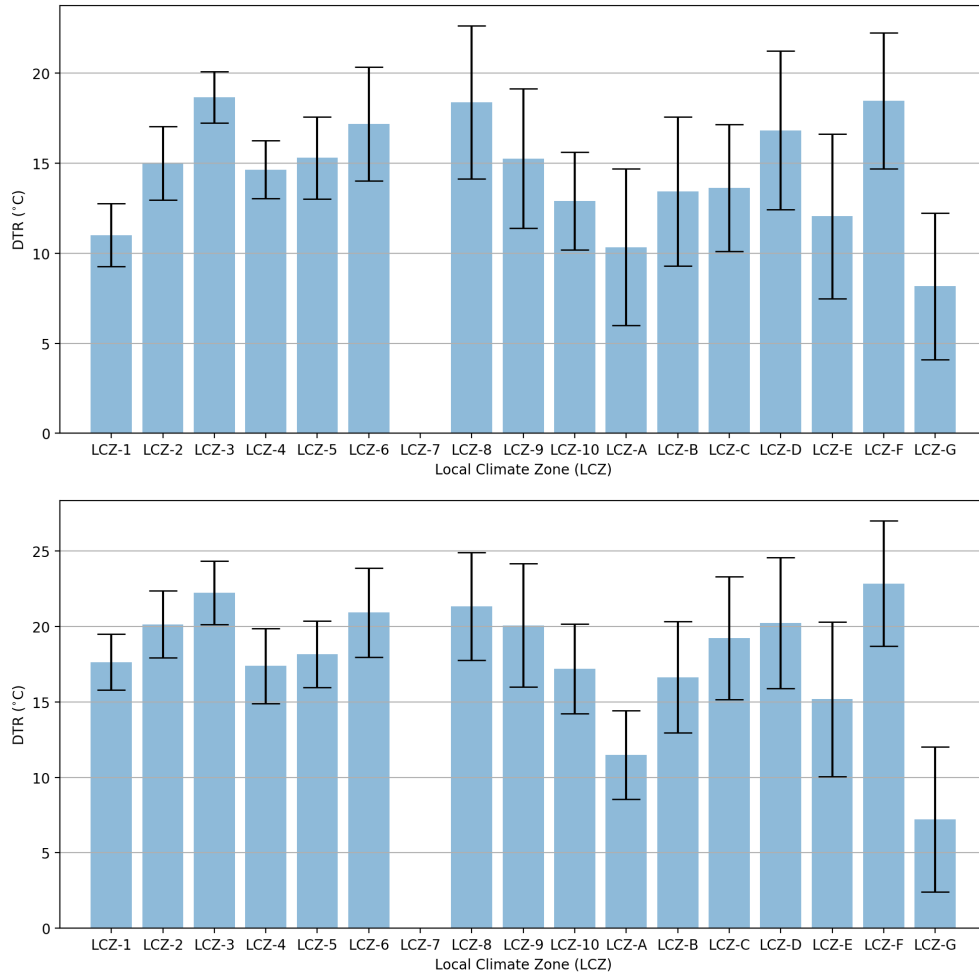
9

Figure 9: Average DTR within each LCZ along with the standard deviation in winter (upper) and summer (lower). No LCZ-7 in the study area.

with a higher population density were exposed to a higher DTR. For census tracts with more than 5,000 persons per km^2, the DTR was 20.3°C, and the DTR for census tracts with less than 1000 persons per km^2 was 18.8°C. Census tracts with higher female populations were with a marginally lower DTR.

Census tracts with more green space (NDVI>0.25) were with a lower DTR, being 18.5°C vs. 20.3°C of the census tracts with limited green space (NDVI between 0.15-0.25). (Cutoffs of 0.15 and 0.25 for NDVI are the 24th and 76th percentiles.) Interestingly, further limited vegetation (NDVI<0.15) resulted in a similar high DTR. A typical example is likely the compact high-rise environment (LCZ-1) mentioned earlier. Lower DTR was observed with a lower PM2.5 concentration. The mean DTR was 18.9°C for census tracts with <12 μg/m^3 PM2.5, and it was 20.1°C for census tracts with >14 μg/m^3 PM2.5. The association of higher DTR and higher PM2.5 may lead to extreme temperature exposure and air pollution exposure at the same time. Finally, the mean DTR was higher for census tracts with a higher percentage of building area, being 20.0°C with more than 30% building area vs. 19.3°C with less than 10% building area.

3.4. Regression results

The crude SMR ranges from zero (due to censoring) to 1.666, with a median of 0.950 and a standard deviation of 0.207. Without considering spatial dependency and covariates, Pearson and Spearman tests (Table 3) indicated that both spatial variability of DTR and mean temperature were positively associated with SMR. Particularly, Pearson
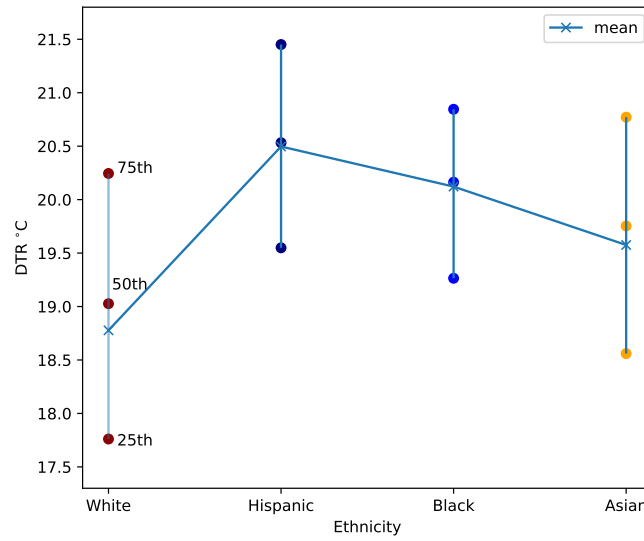
Figure 10: Population weighted exposure to DTR across ethnicity. The connected line is the mean values, and the three points of each ethnicity are the 25th, 50th, and 75th percentiles.
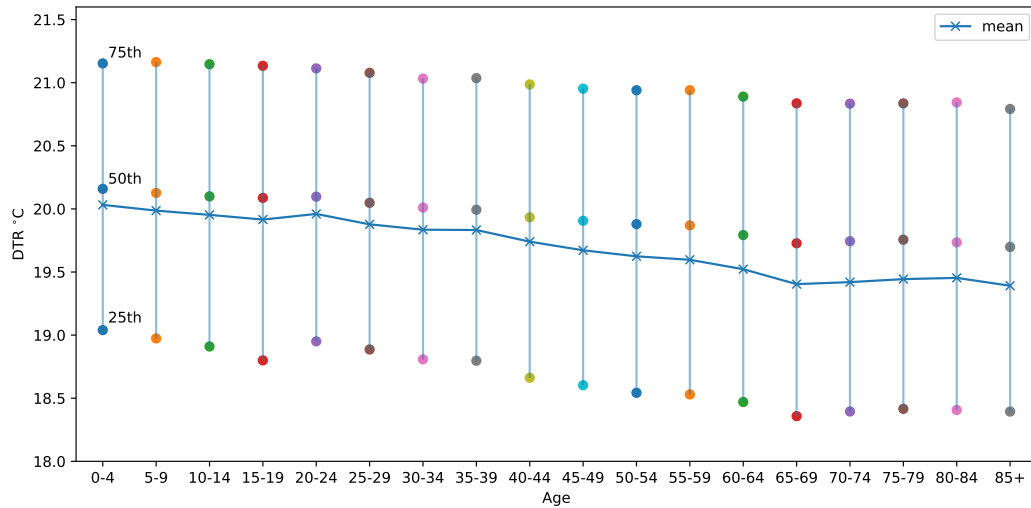

Figure 11: (This figure has been updated.) Population weighted exposure to DTR across age. The connected line is the mean values, and the three points of each ethnicity are the 25th, 50th, and 75th percentiles.

correlations for DTR and mean temperature were r=0.470 and r=0.225, respectively. Other significant variables in both Pearson and Spearman correlations were all negative, including income, percentage of age>65, and percentage of white.

The results of non-spatial and spatial regressions are shown in Table 4. There was no evidence of multicollinearity with the largest VIF of 2.8. The results of spatial variability of mean temperature became insignificant after controlling for spatial dependency and covariates in our study. Spatial variability of DTR was positively associated with all-cause mortality. For areas with DTR > 50th percentile (17.85°C), compared to areas with DTR < 50th percentile in our study, the RR was 1.047 (95% CrI 1.013-1.082).

We show the residuals not explained by the covariates in the fully adjusted model in Figure 13. The residuals are small for most areas. Only three areas are with residuals higher than 0.9, and they all are university campuses
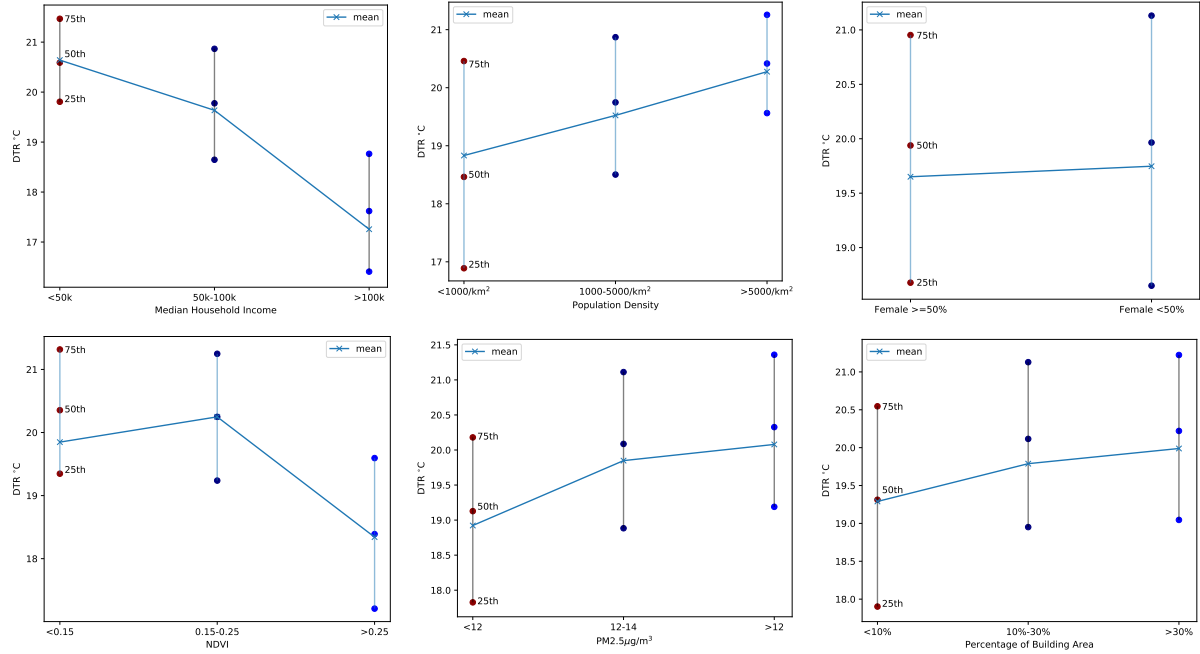
Figure 12: Exposure to DTR of census tracts across median household income, population density, percentage of female populations, green space (NDVI), PM2.5, and percentage of building area. The connected line is the mean values, and the three points of each ethnicity are the 25th, 50th, and 75th percentiles.

Table 3: Correlations between variables and standardized mortality ratio (SMR)

Variable	Mean (SD)	Pearson r	Spearman r_s
DTR	18.954 (2.594)	0.470***	0.532***
Temperature	21.893 (1.240)	0.225***	0.349***
Income	6.906 (2.739)	-0.466***	-0.520***
Age>65 %	13.153 (6.260)	-0.286***	-0.419***
White %	37.258 (24.939)	-0.425***	-0.495***
Female %	50.798 (2.800)	-0.199***	-0.150**
PM2.5	12.782 (2.234)	-0.077	-0.005
Green Space	2.174 (0.829)	-0.367***	-0.374***
Population Density	0.307 (0.246)	0.080	0.101*
Building Area %	16.373 (10.543)	0.057	0.067

1. *p<0.05, **p<0.01, ***p<0.001

2. DTR, Temperature: per °C; Income: per 10,000 US$; Age> 65, White %, Female %, Building Area %: per 1%; PM2.5: per μg/m^3; Green Space: per 0.1 NDVI; Population Density: per 100 m^3.

Table 4: Results of the regression models with different adjustment levels. Data are relative risk estimate.

	non-spatial		spaital	
DTR	1.163 (1.122-1.205)	1.071 (1.034-1.108)	1.054 (1.017-1.090)	1.047 (1.013-1.082)
Temperature	1.005 (0.988-1.022)	0.992 (0.976-1.008)	1.040 (1.023-1.058)	1.015 (0.996-1.034)
Income		0.966 (0.958-0.974)		0.970 (0.963-0.978)
Age>65 %		0.992 (0.989-0.994)		0.994 (0.992-0.996)
White %		1.000 (0.999-1.001)		1.000 (0.999-1.001)
Female %		1.003 (0.996-1.009)		1.000 (0.995-1.006)
PM2.5		0.996 (0.989-1.004)		1.003 (0.995-1.010)
Green Space		0.955 (0.934-0.976)		0.993 (0.969-1.016)
Population Density		0.797 (0.716-0.878)		0.931 (0.850-1.013)
Building Area %		0.998 (0.996-1.000)		0.998 (0.996-1.001)
DIC	3437.35	3400.29	3342.30	3315.66
WAIC (AIC)	3384.64	3370.37	3303.22	3289.84

DTR: high vs. low; Temperature: per °C; Income: per 10,000 US$; Age>65 %, White %, Female %, Building Area %: per 1%; PM2.5: per $\mu g/m^3$; Green Space: per 0.1 NDVI; Population Density: per 100 m^3. DIC: Deviance Information Criterion; WAIC: Watanabe–Akaike information criterion.

as circled in red in Figure 13. The unique population compositions explain the under-fitting in these areas. Three areas are with residuals between 0.3-0.9; these areas are with small populations (<2000). One area is with a residual between 0.2-0.3, and all other areas are with residuals smaller than 0.2. The residual map confirms that the model is valid and explains most mortality risks.

3.5. Sensitivity analysis

3.5.1. Brightness temperature vs. air temperature

We conducted a sensitivity analysis comparing brightness temperature used in this study with air temperature. Hourly air temperature data were extracted from the meteostat package with data from National Oceanic and Atmospheric Administration (NOAA). Brightness and air temperature data were matched with the closest ones in time. The scatter plots with regression results are shown in Figure 14. Overall, brightness temperature (T_b) and air temperature (T_a) have a strong linear correlation (r=0.75-0.91). The correlation is stronger in daytime than at night. Although the absolute values are different, since DTR is a relative value that is the difference between maximum and minimum temperature, the usage of brightness temperature should be justified as it is linearly correlated with air temperature which is equivalent in the model. The variation, apart from their inherit difference, may be explained by the inconsistent observation time between air temperature and brightness temperature, as the air temperature data are hourly. Yet, as brightness temperature (one type of land surface temperature) provides continuous observation values over the spatial domain, usage of these types of data in health studies have been discussed and encouraged to tackle the environmental justice issues (White-Newsome et al., 2013).

3.5.2. Results using continuous DTR

Our study used categorical DTR, which can capture nonlinear association compared to using continuous DTR. This is a practice often used in environmental health studies (Helbich et al., 2018). We conducted a separate analysis, treating DTR as a continuous variable. The result shows an increase of 0.011 in RR per 1°C increase in DTR (RR: 1.011, 95% CrI 1.002-1.019).

4. Discussion

This study examined the spatial heterogeneity of DTR in Los Angeles, one of the megacities with the largest DTR and highest effects of DTR on nonaccidental mortality in the US (Lim et al., 2015). Using LISA, we found that in winter, areas along the highways were with a higher DTR. The two clusters with a high DTR were Commerce in East LA and Anaheim City of Orange County. Coastal areas and mountains were with a low DTR. In summer, the coastal
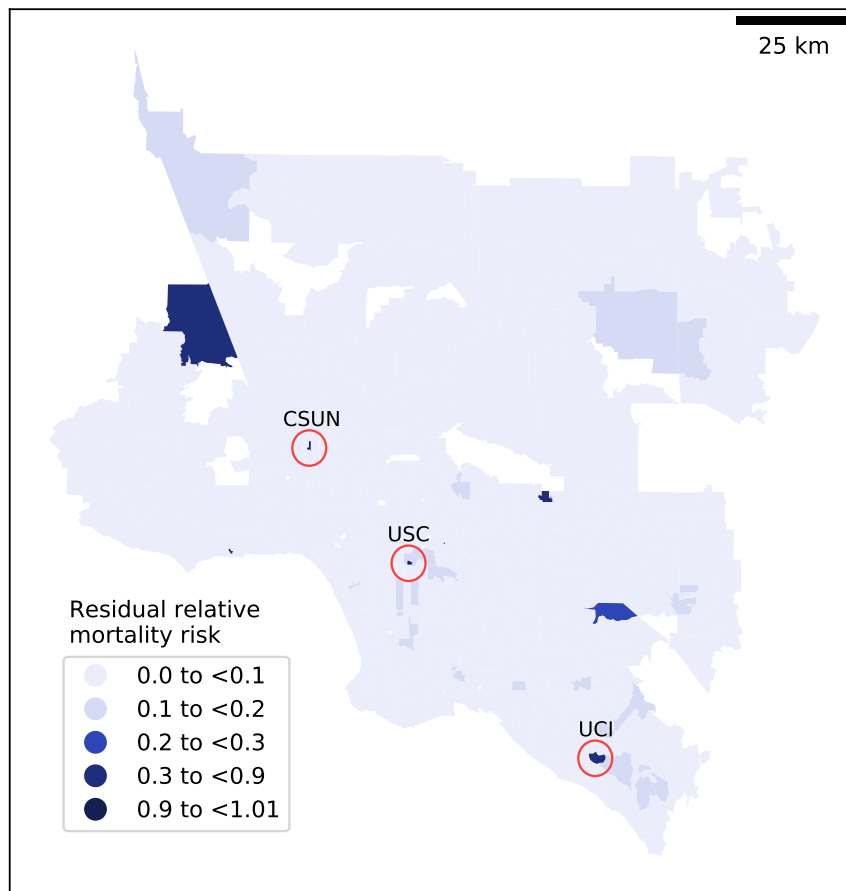
Figure 13: Residuals of the fully adjusted spatial model. Three areas circled in red are with residuals larger than 0.9, and all are university campuses with unique population compositions.
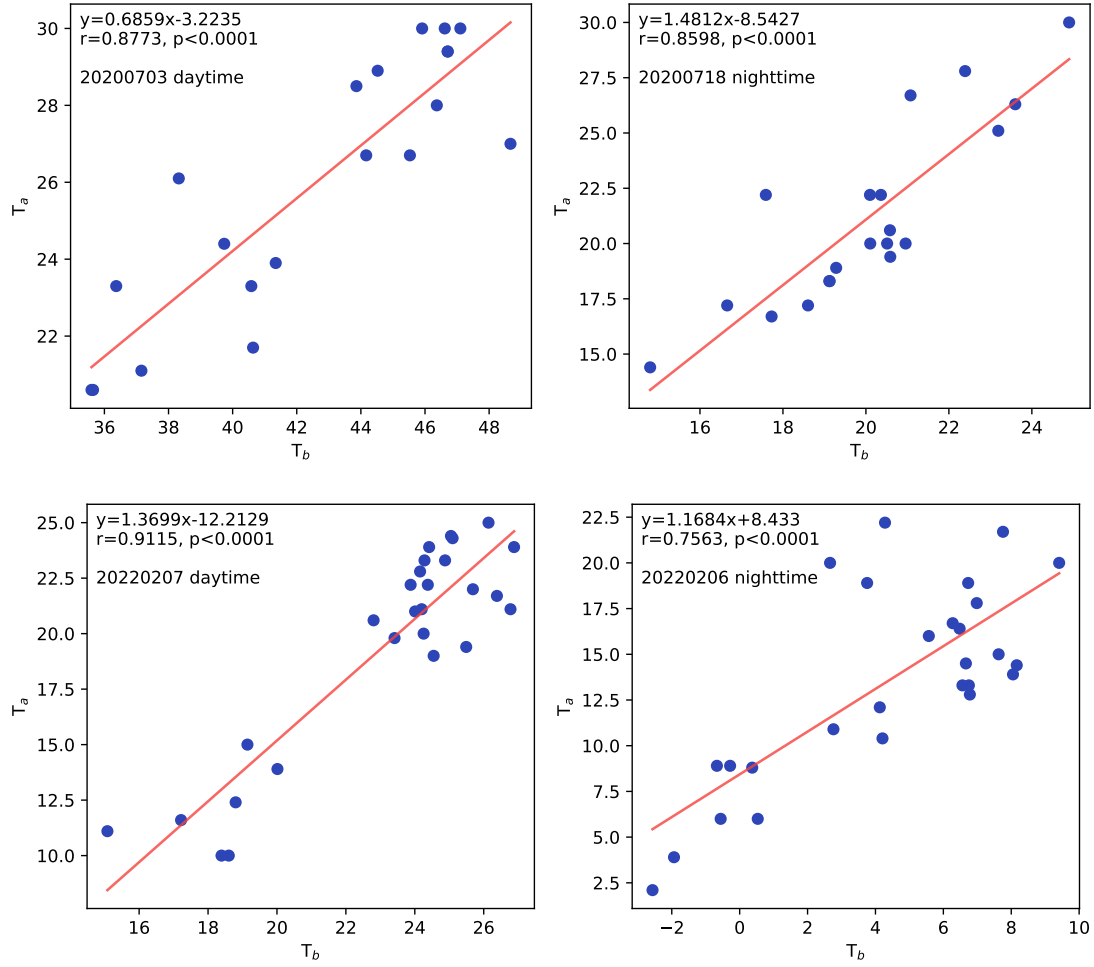
Figure 14: Sensitivity analysis: brightness temperature (T_b) vs. air temperature (T_a)

area stayed cool, and three clusters within the two valleys of Los Angeles (San Bernardino and San Gabriel) were with high temperatures both daytime and nighttime compared to other areas.

We examined the association between DTR and the built environment using the LCZ framework. Within compact LCZs, LCZ-3 compact low-rise was with the highest DTR. Within open LCZs, LCZ-6 was with the highest DTR. While natural LCZs were with a lower DTR, in urban areas, high-rise was associated with a lower DTR.

DTR exposure was disproportionate across subpopulations. Higher mean DTRs were found in census tracts with higher proportions of Hispanic populations. White as a group was exposed to the lowest DTR. Black and Asian were somewhere in between. Higher DTR exposures were found among young populations. Age group 0-4 was with the highest DTR exposure. Census tracts with a lower median household income (<US$50,000) were with a higher DTR (20.6°C), which was the highest among all subpopulations. A higher DTR was also found in census tracts with a higher population density, less green space (lower NDVI), higher PM2.5 concentration, and a higher percentage of building areas. For zip code areas with a higher DTR compared to those with a lower DTR, the relative risk of mortality is 1.047 (CrI 1.013-1.082), as estimated using the fully-adjusted spatial Bayesian Poisson regression model.

4.1. Strength of this study

Advancing from other studies, our study examined not only the neighborhood-level temperature but also the spatial variability of DTR. To the best of our knowledge, the presented study is the first to investigate the spatial association

15

between DTR and mortality at the neighborhood scale. This provided a novel insight regarding how daily temperature variations could affect community health risks within a city. Particularly, previous studies have found that short-term exposure to temperature variations (such as DTR) can influence mortality risk worldwide (Yang et al., 2018; Zhang et al., 2018; Lee et al., 2020). This study further indicated that the variations of temperature exposure within a day as the long-term exposure can increase mortality risk for an individual in the long run.

There are several potential reasons and pathways on how DTR affects mortality/morbidity, primarily through our cardiovascular and respiratory systems (Cheng et al., 2014). DTR could increase the blood catecholamine level by stimulating skin receptors, increasing heart rate, blood pressure, and oxygen consumption (Liang et al., 2008; Lim et al., 2013). DTR could cause desquamation of mucosal epithelial cells that could be amplified by rhinitis (Graudenz et al., 2006). This risk could be higher for children having asthma with under-developed immune systems (Xu et al., 2013a). Childhood diarrhea was also associated with increased DTR that could be explained by the changing immune system caused by short-time weather change (Bull, 1980; Xu et al., 2013b). Indirectly, DTR could also enhance the transmission of virus, resulting in exacerbations of respiratory diseases (Onozuka, 2015).

The results can be explained by medical implications as well as results from our heat vulnerability analysis. Our LULC analysis indicated the LCZ with the highest DTR values were compact low-rise areas with limited green space. This is an important finding, as most of the compact low-rise areas in the United States are two/multi-storey apartments with low-income facilities (Berger et al., 2022). These types of housing usually have poor environmental hygiene and building design. Most of them can be without air-conditioning. When high DTR occurs, indoor exposure can be extreme and affect human health at night. Such a problem is critical, as DTR usually affects human health risk by weakening the acclimatization of an individual due to large variations of heat exposure. Combined with the factor of poor housing conditions that can not mitigate climatic risk, frequent exposure to large DTR can be fatal to vulnerable subpopulations.

The results regarding spatial associations and neighborhood environment and DTR also supported the above findings. Specifically, low-income, young-age, and non-white populations were found to be exposed to higher DTRs. For the non-white population in Los Angles, a high proportion of them were low-income individuals with poor housing conditions, especially for Hispanics (Hsu et al., 2021). A typical area for this is East Los Angeles (Padua and Doran, 2016). Low-income and low-education individuals usually have low affordability for disaster preparedness and low health literacy for risk reduction (Chen et al., 2020). The integration of poor housing conditions and population vulnerability could enlarge their risk from temperature extremes. This may be the reason why neighborhoods with frequent long-term exposure to large DTR were associated with higher all-cause mortality in Los Angles in our study.

For young-age such as infants, it is well recognized that these individuals are highly vulnerable to temperature extremes due to the low ability of self-protection (Basagaña et al., 2011; Auger et al., 2015). The infants may not appropriately recognize the important change in body status (e.g., change of body temperature, dehydration) or may not know how to reduce or mitigate the health issues from these changes (Basagaña et al., 2011). As a result, their frequent exposure to large DTR could be a recurring risk factor that affects their health throughout the years.

Based on these results, our study therefore recognized the underestimated risk from long-term exposure to DTR, as frequently exposing large temperature variations in a year could be a recurring risk factor among vulnerable subpopulations. The risk could be further increased due to poor housing/neighborhood conditions and low health literacy.

4.2. Limitations

Some limitations should be noted. Death counts smaller than 11 were censored in the dataset, leading to underestimating deaths in these zip code areas. However, the number of censored sites was small since we used all-cause mortality. We used two pairs of Landsat imagery to estimate the long-term DTR, which may not be representative of the study period. Yet using cloudless satellite image snapshots is likely the only way to capture the spatial heterogeneity of DTR. Brightness Temperature is different from apparent temperature as perceived by humans. However, the subtraction to calculate DTR should minimize the difference between Brightness Temperature and apparent temperature. We did not observe a significant association between mean temperature and mortality, which may be due to the limited temporal resolution of satellite data, as continuous observation is not possible yet due to limitations of satellite data and cloud conditions. The study units of census tracts and zip code areas disregard the life course exposure of individuals. Confounding cannot be precluded. Finally, although examining the spatial heterogeneity of the association between DTR and mortality within a megacity is valuable, causality cannot be inferred.

5. Conclusions

This study evaluated the spatial variability of DTR and its association with LCZ, neighborhood environment and all-cause mortality in Los Angeles, United States. Our results highlighted a significant association between neighborhood-level DTR and all-cause mortality, while neighborhoods with frequent long-term exposure to large DTR could be compact low-rise areas and with vulnerable sub-populations (e.g., infants, minorities). Our results implied that housing conditions and neighborhood design should be further improved to minimize risk from DTR exposure in order to increase climate resilience among at-risk neighborhoods with vulnerable sub-populations in the mega-cities with mixed populations.

Acknowledgements

References

Anderson, B.G., Bell, M.L., 2009. Weather-related mortality: how heat, cold, and heat waves affect mortality in the united states. Epidemiology (Cambridge, Mass.) 20, 205.

Anselin, L., 1995. Local indicators of spatial association—lisa. Geographical analysis 27, 93–115.

Anselin, L., Syabri, I., Kho, Y., 2009. Geoda: an introduction to spatial data analysis, in: Handbook of applied spatial analysis: Software tools, methods and applications. Springer, pp. 73–89.

Auger, N., Fraser, W.D., Smargiassi, A., Kosatsky, T., 2015. Ambient heat and sudden infant death: a case-crossover study spanning 30 years in montreal, canada. Environmental health perspectives 123, 712–716.

Basagaña, X., Sartini, C., Barrera-Gómez, J., Dadvand, P., Cunillera, J., Ostro, B., Sunyer, J., Medina-Ramón, M., 2011. Heat waves and cause-specific mortality at all ages. Epidemiology , 765–772.

Berg, E., Kucharik, C., 2021. The dynamic relationship between air and land surface temperature within the madison, wisconsin urban heat island. Remote Sensing 14, 165.

Berger, T., Chundeli, F.A., Pandey, R.U., Jain, M., Tarafdar, A.K., Ramamurthy, A., 2022. Low-income residents' strategies to cope with urban heat. Land Use Policy 119, 106192.

Besag, J., York, J., Mollié, A., 1991. Bayesian image restoration, with two applications in spatial statistics. Annals of the institute of statistical mathematics 43, 1–20.

Bull, G., 1980. The weather and deaths from pneumonia. The Lancet 315, 1405–1408.

Cao, L., Li, P., Zhang, L., Chen, T., 2008. Remote sensing image-based analysis of the relationship between urban heat island and vegetation fraction. The International Archives of the Photogrammetry, Remote Sensing and Spatial Information Sciences 37, 1379–1384.

Chen, M., Ban-Weiss, G.A., Sanders, K.T., 2020. Utilizing smart-meter data to project impacts of urban warming on residential electricity use for vulnerable populations in southern california. Environmental Research Letters 15, 064001.

Chen, T.L., Lin, H., Chiu, Y.H., 2022. Heat vulnerability and extreme heat risk at the metropolitan scale: A case study of taipei metropolitan area, taiwan. Urban Climate 41, 101054.

Chen, X.L., Zhao, H.M., Li, P.X., Yin, Z.Y., 2006. Remote sensing image-based analysis of the relationship between urban heat island and land use/cover changes. Remote sensing of environment 104, 133–146.

Cheng, J., Xu, Z., Zhu, R., Wang, X., Jin, L., Song, J., Su, H., 2014. Impact of diurnal temperature range on human health: a systematic review. International journal of biometeorology 58, 2011–2024.

Demuzere, M., Kittner, J., Martilli, A., Mills, G., Moede, C., Stewart, I.D., van Vliet, J., Bechtel, B., 2022. A global map of local climate zones to support earth system modelling and urban scale environmental science. Earth System Science Data Discussions , 1–57.

Dinda, S., 2004. Environmental kuznets curve hypothesis: a survey. Ecological economics 49, 431–455.

Du, C., Ren, H., Qin, Q., Meng, J., Zhao, S., 2015. A practical split-window algorithm for estimating land surface temperature from landsat 8 data. Remote sensing 7, 647–665.

García-Pérez, J., Fernández-Navarro, P., Castelló, A., López-Cima, M.F., Ramis, R., Boldo, E., Lopez-Abente, G., 2013. Cancer mortality in towns in the vicinity of incinerators and installations for the recovery or disposal of hazardous waste. Environment international 51, 31–44.

Gasparrini, A., Guo, Y., Hashizume, M., Lavigne, E., Zanobetti, A., Schwartz, J., Tobias, A., Tong, S., Rocklöv, J., Forsberg, B., et al., 2015. Mortality risk attributable to high and low ambient temperature: a multicountry observational study. The lancet 386, 369–375.

Geletič, J., Lehnert, M., Savić, S., Milošević, D., 2019. Inter-/intra-zonal seasonal variability of the surface urban heat island based on local climate zones in three central european cities. Building and Environment 156, 21–32.

Graudenz, G.S., Landgraf, R.G., Jancar, S., Tribess, A., Fonseca, S.G., Faé, K.C., Kalil, J., 2006. The role of allergic rhinitis in nasal responses to sudden temperature changes. Journal of allergy and clinical immunology 118, 1126–1132.

Helbich, M., De Beurs, D., Kwan, M.P., O'Connor, R.C., Groenewegen, P.P., 2018. Natural environments and suicide mortality in the netherlands: a cross-sectional, ecological study. The Lancet Planetary Health 2, e134–e139.

Ho, H.C., Knudby, A., Chi, G., Aminipouri, M., Lai, D.Y.F., 2018. Spatiotemporal analysis of regional socio-economic vulnerability change associated with heat risks in canada. Applied Geography 95, 61–70.

Hsu, A., Sheriff, G., Chakraborty, T., Manya, D., 2021. Disproportionate exposure to urban heat island intensity across major us cities. Nature communications 12, 1–11.

Johnson, D.P., Wilson, J.S., 2009. The socio-spatial dynamics of extreme urban heat events: The case of heat-related deaths in philadelphia. Applied geography 29, 419–434.

Kan, H., London, S.J., Chen, H., Song, G., Chen, G., Jiang, L., Zhao, N., Zhang, Y., Chen, B., 2007. Diurnal temperature range and daily mortality in shanghai, china. Environmental research 103, 424–431.

Kim, J., Shin, J., Lim, Y.H., Honda, Y., Hashizume, M., Guo, Y.L., Kan, H., Yi, S., Kim, H., 2016. Comprehensive approach to understand the association between diurnal temperature range and mortality in east asia. Science of the Total Environment 539, 313–321.

Kuznets, S., 1955. Economic growth and income inequality. The American Economic Review 45, 1–28.

Lee, W., Bell, M.L., Gasparrini, A., Armstrong, B.G., Sera, F., Hwang, S., Lavigne, E., Zanobetti, A., Coelho, M.d.S.Z.S., Saldiva, P.H.N., et al., 2018. Mortality burden of diurnal temperature range and its temporal changes: a multi-country study. Environment international 110, 123–130.

Lee, W., Kim, Y., Sera, F., Gasparrini, A., Park, R., Choi, H.M., Prifti, K., Bell, M.L., Abrutzky, R., Guo, Y., et al., 2020. Projections of excess mortality related to diurnal temperature range under climate change scenarios: a multi-country modelling study. The Lancet Planetary Health 4, e512–e521.

Lee, W.H., Lim, Y.H., Dang, T.N., Seposo, X., Honda, Y., Guo, Y.L.L., Jang, H.M., Kim, H., 2017. An investigation on attributes of ambient temperature and diurnal temperature range on mortality in five east-asian countries. Scientific reports 7, 1–9.

Leroux, B.G., Lei, X., Breslow, N., 2000. Estimation of disease rates in small areas: a new mixed model for spatial dependence, in: Statistical models in epidemiology, the environment, and clinical trials. Springer, pp. 179–191.

Liang, W.M., Liu, W.P., Chou, S.Y., Kuo, H.W., 2008. Ambient temperature and emergency room admissions for acute coronary syndrome in taiwan. International journal of biometeorology 52, 223–229.

Lim, Y.H., Kim, H., Kim, J.H., Bae, S., Hong, Y.C., 2013. Effect of diurnal temperature range on cardiovascular markers in the elderly in seoul, korea. International Journal of Biometeorology 57, 597–603.

Lim, Y.H., Reid, C.E., Mann, J.K., Jerrett, M., Kim, H., 2015. Diurnal temperature range and short-term mortality in large us communities. International journal of biometeorology 59, 1311–1319.

Mirzaei, P.A., 2015. Recent challenges in modeling of urban heat island. Sustainable cities and society 19, 200–206.

Muthukumar, P., Cocom, E., Nagrecha, K., Comer, D., Burga, I., Taub, J., Calvert, C.F., Holm, J., Pourhomayoun, M., 2022. Predicting pm2. 5 atmospheric air pollution using deep learning with meteorological data and ground-based observations and remote-sensing satellite big data. Air Quality, Atmosphere & Health 15, 1221–1234.

Niclòs, R., Puchades, J., Coll, C., Barberà, M.J., Pérez-Planells, L., Valiente, J.A., Sánchez, J.M., 2021. Evaluation of landsat-8 tirs data recalibrations and land surface temperature split-window algorithms over a homogeneous crop area with different phenological land covers. ISPRS Journal of Photogrammetry and Remote Sensing 174, 237–253.

O'Brien, D.T., Gridley, B., Trlica, A., Wang, J.A., Shrivastava, A., 2020. Urban heat islets: Street segments, land surface temperatures, and medical emergencies during heat advisories. American Journal of Public Health 110, 994–1001.

Onozuka, D., 2015. The influence of diurnal temperature range on the incidence of respiratory syncytial virus in japan. Epidemiology & Infection 143, 813–820.

Padua, L.A., Doran, J.K., 2016. From being unbanked to becoming unbanked or unbankable: Community experts describe financial practices of latinos in east los angeles. Journal of Community Practice 24, 428–444.

Pelta, R., Chudnovsky, A.A., 2017. Spatiotemporal estimation of air temperature patterns at the street level using high resolution satellite imagery. Science of the Total Environment 579, 675–684.

Pelta, R., Chudnovsky, A.A., Schwartz, J., 2016. Spatio-temporal behavior of brightness temperature in tel-aviv and its application to air temperature monitoring. Environmental Pollution 208, 153–160.

Ponjoan, A., Blanch, J., Alves-Cabratosa, L., Lluch, R.M., Comas-Cufí, M., Parramon, D., García-Gil, M.M., Ramos, R., Petersen, I., 2021. Extreme diurnal temperature range and cardiovascular emergency hospitalisations in a mediterranean region. Occupational and Environmental Medicine 78, 62–68.

Reid, C.E., Considine, E.M., Maestas, M.M., Li, G., 2021. Daily pm2. 5 concentration estimates by county, zip code, and census tract in 11 western states 2008–2018. Scientific data 8, 1–15.

Rosenthal, J.K., Kinney, P.L., Metzger, K.B., 2014. Intra-urban vulnerability to heat-related mortality in new york city, 1997–2006. Health & place 30, 45–60.

Sabrin, S., Karimi, M., Fahad, M.G.R., Nazari, R., 2020. Quantifying environmental and social vulnerability: Role of urban heat island and air quality, a case study of camden, nj. Urban Climate 34, 100699.

Sekertekin, A., Bonafoni, S., 2020. Sensitivity analysis and validation of daytime and nighttime land surface temperature retrievals from landsat 8 using different algorithms and emissivity models. Remote Sensing 12, 2776.

Sharafkhani, R., Khanjani, N., Bakhtiari, B., Jahani, Y., Mahdi, R.E., 2017. Diurnal temperature range and mortality in urmia, the northwest of iran. Journal of thermal biology 69, 281–287.

Shi, L., Kloog, I., Zanobetti, A., Liu, P., Schwartz, J.D., 2015. Impacts of temperature and its variability on mortality in new england. Nature climate change 5, 988–991.

Singh, A., Pathak, P.K., Chauhan, R.K., Pan, W., 2011. Infant and child mortality in india in the last two decades: a geospatial analysis. Plos one 6, e26856.

Smargiassi, A., Goldberg, M.S., Plante, C., Fournier, M., Baudouin, Y., Kosatsky, T., 2009. Variation of daily warm season mortality as a function of micro-urban heat islands. Journal of Epidemiology & Community Health 63, 659–664.

Sobstyl, J., Emig, T., Qomi, M.A., Ulm, F.J., Pellenq, R.M., 2018. Role of city texture in urban heat islands at nighttime. Physical review letters 120, 108701.

Son, J.Y., Liu, J.C., Bell, M.L., 2019. Temperature-related mortality: a systematic review and investigation of effect modifiers. Environmental Research Letters 14, 073004.

Stewart, I.D., Oke, T.R., 2012. Local climate zones for urban temperature studies. Bulletin of the American Meteorological Society 93, 1879–1900.

Stewart, I.D., Oke, T.R., Krayenhoff, E.S., 2014. Evaluation of the 'local climate zone'scheme using temperature observations and model simulations. International journal of climatology 34, 1062–1080.

Thach, T.Q., Zheng, Q., Lai, P.C., Wong, P.P.Y., Chau, P.Y.K., Jahn, H.J., Plass, D., Katzschner, L., Kraemer, A., Wong, C.M., 2015. Assessing spatial associations between thermal stress and mortality in hong kong: a small-area ecological study. Science of the Total Environment 502, 666–672.

Thorpe, L.E., Chunara, R., Roberts, T., Pantaleo, N., Irvine, C., Conderino, S., Li, Y., Hsieh, P.Y., Gourevitch, M.N., Levine, S., et al., 2022. Building public health surveillance 3.0: Emerging timely measures of physical, economic, and social environmental conditions affecting health. American journal of public health 112, 1436–1445.

Wan, Z., Dozier, J., 1996. A generalized split-window algorithm for retrieving land-surface temperature from space. IEEE Transactions on geoscience and remote sensing 34, 892–905.

White-Newsome, J.L., Brines, S.J., Brown, D.G., Dvonch, J.T., Gronlund, C.J., Zhang, K., Oswald, E.M., O'Neill, M.S., 2013. Validating satellite-derived land surface temperature with in situ measurements: A public health perspective. Environmental health perspectives 121, 925–931.

Wilson, B., Porter, J.R., Kearns, E.J., Hoffman, J.S., Shu, E., Lai, K., Bauer, M., Pope, M., 2022. High-resolution estimation of monthly air temperature from joint modeling of in situ measurements and gridded temperature data. Climate 10, 47.

Xu, Z., Huang, C., Su, H., Turner, L.R., Qiao, Z., Tong, S., 2013a. Diurnal temperature range and childhood asthma: a time-series study. Environmental health 12, 1–5.

Xu, Z., Huang, C., Turner, L.R., Su, H., Qiao, Z., Tong, S., 2013b. Is diurnal temperature range a risk factor for childhood diarrhea? PLoS One 8, e64713.

Yang, J., Zhou, M., Li, M., Yin, P., Wang, B., Pilot, E., Liu, Y., van der Hoek, W., van Asten, L., Krafft, T., et al., 2018. Diurnal temperature range in relation to death from stroke in china. Environmental research 164, 669–675.

Yang, Y., Song, F., Ma, J., Wei, Z., Song, L., Cao, W., 2022. Spatial and temporal variation of heat islands in the main urban area of zhengzhou under the two-way influence of urbanization and urban forestry. Plos one 17, e0272626.

Yin, C., Yuan, M., Lu, Y., Huang, Y., Liu, Y., 2018. Effects of urban form on the urban heat island effect based on spatial regression model. Science of the Total Environment 634, 696–704.

Zhang, Y., Peng, M., Wang, L., Yu, C., 2018. Association of diurnal temperature range with daily mortality in england and wales: a nationwide time-series study. Science of the Total Environment 619, 291–300.

Zhao, L., Lee, X., Smith, R.B., Oleson, K., 2014. Strong contributions of local background climate to urban heat islands. Nature 511, 216–219.